Journal of Power Sources 264 (2014) 35–41

Contents lists available at ScienceDirect

Journal of Power Sources

journal homepage: www.elsevier.com/locate/jpowsour

Improved properties of dye-sensitized solar cells by multifunctional scattering layer of yolk-shell-like TiO_2 microspheres

Kaimo Guo, Meiya Li*, Xiaoli Fang, Lihua Bai, Mengdai Luoshan, Fuping Zhang, Xingzhong Zhao

School of Physics and Technology, The Key Laboratory of Artificial Micro/Nano Structures of Ministry of Education, Wuhan University, Wuhan 430072, PR China

HIGHLIGHTS

- Novel yolk-shell TiO_2 hierarchical microsphere (YSTHS) photoanode was prepared.
- The properties of the DSSC with YSTHS photoanode were significantly improved.
- The increase of J_{sc} and η were attributed to the enhancement of light scattering and dye adsorption.
- The enhanced light scattering and dye adsorption were ascribed to the unique structure of the YSTHS.

ARTICLE INFO

Article history:
Received 27 February 2014
Received in revised form
30 March 2014
Accepted 13 April 2014
Available online 26 April 2014

Keywords:
Yolk-shell-like TiO_2 hierarchical microspheres
Heterostructure bilayer photoanode
Dye-sensitized solar cells
Light scattering
Dye adsorption

ABSTRACT

Novel yolk-shell-like TiO_2 hierarchical microspheres (YSTHSs) were synthesized by a facile one-pot hydrothermal method. These YSTHSs exhibited excellent light scattering ability and high specific surface area for more dye adsorption. A YSTHSs multifunctional scattering layer was fabricated on top of a conventional TiO_2 nanocrystalline layer (T) to form a heterostructure bilayer photoanode (T-YSTHS). The influences of the YSTHSs on the properties of the photoanode and dye-sensitized solar cell (DSSC) were investigated. Studies indicated that by introducing the YSTHSs, the light scattering, dye loading, electron mobility and lifetime of this bilayer photoanode were remarkably increased, resulting in the great enhancement in the short-circuit current density (J_{sc}) and thus the photoelectric conversion efficiency (PCE) of the DSSCs. This T-YSTHS based DSSC exhibited the maximum J_{sc} of 16.35 mA cm^{-2} and PCE of 6.01%, remarkably higher than those of the conventional TiO_2 nanocrystalline (2T)-based DSSC by 27.1% and 20.4%, respectively. The remarkable enhancement in J_{sc} and PCE for the T-YSTHS-based DSSC compared to the 2T-based DSSCs are mainly attributed to the significant enhancement in light scattering and the increase in the specific surface area for dye adsorption due to the unique yolk-shell hierarchical microsphere structure of the YSTHSs.

1. Introduction

The fossil fuels crisis and global warming resulted from rapid increases in population and industrial activity worldwide are considered as one of the biggest challenges facing humanity today. Considerable efforts have been made toward creating environmentally and economically viable new energy. Of which, solar cells have emerged as one of the most promising new candidates in the area of renewable energy. Since the pioneering work done by O'Regan and Grätzel in 1991 [1], dye-sensitized solar cells (DSSCs), a third-generation solar cell with the most promising to replace conventional photovoltaic devices (such as silicon-based solar cells), have draw significant attention due to their low manufacturing cost, facile fabrication processes and relatively high power conversion efficiencies [2–4]. A typical DSSC device is structurally comprised of a nanocrystalline TiO_2 photoanode film onto which a monolayer of dye molecules is adsorbed, a redox electrolyte and a counter electrode in a sandwich structure. In order to obtain high photoelectric conversion efficiency in DSSCs, many research efforts, including making the TiO_2 photoanodes with various morphologies and textures [5–8] (such as nanorods [9], nanotube [10], nanosheets [11], mesoporous beads [12]), dopants [13–15], synthesizing new redox shuttles [16] and dyes capable of effectively absorbing visible and near-infrared light [17]

* Corresponding author.
E-mail address: myli@whu.edu.cn (M. Li).

http://dx.doi.org/10.1016/j.jpowsour.2014.04.061
0378-7753/

have been conducted over the past few years. As a key part of DSSCs, the photoanode, which is conventionally made of TiO_2 nanocrystals (~20 nm in diameter) porous film with a high specific surface area and responsible for dye-loading, light-absorption, photoelectron generating and transfer, plays a critical role in determining the final photoelectric conversion efficiency. Thus, it is essential to design and fabricate a efficient photoanode for obtaining high photoelectric conversion efficiency in DSSCs. However, the conventional TiO_2 photoanode film usually exhibits high transparency and weak light scattering due to the nanometer particle size, resulting in poor light-harvesting efficiency (LHE) [8,18]. To tackle this issue, the concept of the bilayer structure with a scattering layer as the overlayer has recently been proposed as it could enhance the LHE by confining the incident light within the photoanode via scattering or diffracting it backward [19,20]. Generally, the scattering layer is made of the solid TiO_2 large particles (STP) of ~400 nm in diameter for improving light scattering, which is usually placed on top of the nanocrystalline TiO_2 layer to form a bilayer photoanode. However, the introduction of such large particles would reduce the dye-loading capacity of the photoanode due to the decrease of the specific surface area, and thus leading to the decrease of the photocurrent, to some extent [20]. Thus, new multifunctional TiO_2 photoanode materials, offering both a good capability for light scattering and a high specific surface area for dye loading, should be synthesized for application to the DSSCs.

Among the various nanostructures of the TiO_2 materials reported recently, hollow TiO_2 nanostructures are considered to be a very promising photoanode material for DSSCs to harvest light efficiently by scattering and reflecting effects while maintaining a relatively high specific surface area for efficient dye adsorption [21,22]. Specially, "yolk-shell" (or so-called "rattle-type") TiO_2 hierarchical microspheres are recently emerging as an interesting new member of the hollow nanoarchitecture family. The unique physical properties of the yolk-shell nanostructures make them attractive materials for applications in catalysis [23], adsorption [24], drug delivery [25], sensing devices [26] and photovoltaic devices [27,28]. However, study on the application of such yolk-shell hierarchical architectures in DSSCs is up to date extremely sparse.

In this study, novel yolk-shell TiO_2 hierarchical microspheres (YSTHSs) with relatively high specific surface area were synthesized by a modified hydrothermal method. These YSTHSs were then used as a multifunctional scattering layer (MSL) over the underlayer TiO_2 nanoparticle film to form a bilayer photoanode for DSSCs. The configuration of the assembled DSSC with such bilayer photoanode is shown schematically in Fig. 1. The influences of the YSTHSs overlayer on the properties of the photoanode and the DSSCs were investigated.

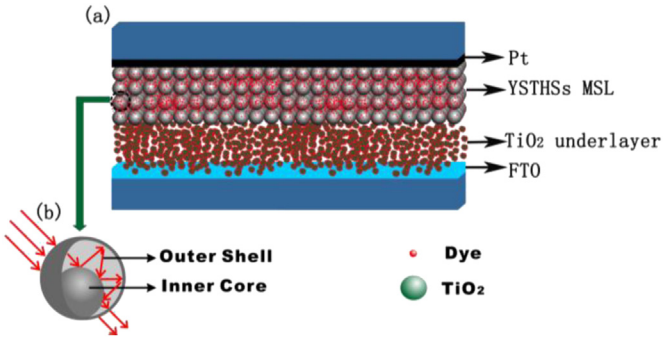

Fig. 1. (a) Schematic structure of the DSSCs incorporated with YSTHSs MSL in TiO_2 photoanode. (b) Cross section of the YSTHS and the light pathway around it.

2. Experimental section

2.1. Materials

The commercial solid TiO_2 large particles (STP, ~400 nm), ethanol (EtOH, 95%), titanium sulfate ($Ti(SO_4)_2$), ammonium fluoride(NH_4F), urea and propylene carbonate (PC) were obtained from Sinopharm Chemical Reagent Co., Ltd. The Ru dye and cis-di(thiocyanato)-bis(2,2′-bipyridyl-4,4′-dicarboxylate) ruthenium(II) (N719) were purchased from Solaronix (Switzerland). The Iodine (I_2, 99.8%) was acquired from Beijing Yili chemicals (China). Lithium iodide (LiI, 99%) and 4-tert-butylpyridine (TBP) were purchased from Acros. The Fluorine–doped SnO_2 conductive glasses (FTO, sheet resistance 10–15 Ω sq^{-1}, Asahi Glass, Japan) were used as the substrate for the TiO_2 photoanode film. All the reagents used were of analytical purity. All water used in this study was deionized (18.2 MΩ, milli-Q pore).

2.2. Preparation of yolk-shell structure TiO_2 microspheres

The YSTHSs were synthesized by a facile one-pot template-free hydrothermal method [23]. In a typical synthesis route, 15 mmol $Ti(SO_4)_2$ was added to the mixture solution of 75 mL ethanol and 75 mL DI-water under vigorous magnetic stirring for 30 min. Subsequently, 15 mmol NH_4F and 30 mol urea were added to the above solution. After stirring for another 30 min, the mixed solution was then transferred to two 100 mL Teflon-lined stainless steel autoclaves, sealed, and hydrothermally treated at 180 °C for 2 h. After cooling to room temperature, the white precipitates of YSTHSs were obtained via centrifugation. The obtained YSTHSs were then used to make the doctor-blading slurry for fabricating the scattering layer on top of the TiO_2 nanocrystalline electrode.

2.3. Fabrication of photoanodes and DSSCs

The TiO_2 paste was made from commercially available TiO_2 nanoparticles (Degussa P25) according to the reported procedure [29]. A conventional nanocrystalline TiO_2 films of about 6 μm (denoted as T) was fabricated by doctor-blading TiO_2 paste on FTO glasses, drying and then annealing at 500 °C for 30 min. To study the influences of STP and YSTHSs on the properties of DSSCs, a conventional scattering layer of large solid TiO_2 particles (STP) and a novel scattering layer of mesoporous YSTHSs were fabricated on top of the above conventional TiO_2 layer by the same doctor-blading process to form the heterostrucutre bilayer photoanode films (~12 μm thick) of T-STP and T-YSTHS, respectively. A conventional TiO_2 photoanode film with about 12 μm thick (denoted as 2T) was fabricated for comparison study. These photoanodes were sensitized by immersing them into the solution of cis-di(thiocyanato)-bis(2,2′-bipyridyl-4,4′-dicarboxylate) ruthenium(II) (N719) with a concentration of 500 μM in the mixture of EtOH and tert-butyl alcohol (volume ratio: 1/1) at 60 °C overnight. Subsequently, these sensitized photoanodes were rinsed with ethanol and dried in an oven at 60 °C for 30 min. These photoanodes and platinized counter electrodes were then assembled to form a series of DSSCs by sandwiching a redox (I^-/I_3^-) electrolyte solution.

2.4. Characterizations

Field-emission scanning electron microscope (SEM, JEOL, 6700F, Japan) and transmission electron microscope (TEM, JEM-2010FEF(UHR)) were applied to observe the morphology and structure of the as-prepared YSTHSs. The crystalline structure of the YSTHSs was determined by X-ray diffraction (XRD, D8 Advance, Bruker, Germany). The pore size distribution and specific surface

area of these samples were analyzed by Brunauer–Emmett–Teller (BET) nitrogen sorption–desorption measurements (JW-BK, China). Diffuse reflection spectra of the photoanode films were obtained on a UV–vis–NIR spectrophotometer (Cary 5000,Varian). The photocurrent–voltage (*J–V*) characteristics of the DSSCs were measured under an irradiance of 100 mW cm^{-2} (AM 1.5 simulated illumination (Newport, 91192, Global)) at an effective irradiated area of 0.25 cm^2. A 300 W xenon lamp (Newport, USA) was used to give incident light ranging from 400 to 800 nm for the incident photo-to-electron conversion efficiency (IPCE) measurements. Electrochemical impedance spectra (EIS) were obtained by a computer-controlled electrochemical workstation CHI660C (Shanghai, China) with a frequency range from 100 kHz to 0.1 Hz in the condition of open circuit under 100 mW cm^{-2} irradiation. The amount of dye loaded on each photoanode was checked by desorbing the dye from the photoanode into 0.1 M NaOH aqueous solution and measuring the UV–Vis absorbance spectra of the dye solution.

3. Results and discussion

3.1. Characterization of the YSTHSs

The SEM images (Fig. 2(a)) illustrate the unique morphology of the YSTHSs in which numerous TiO_2 microspheres with hierarchical structure can be observed clearly. The diameters of these YSTHSs are in the range of 3–5 μm. Moreover, the cracked microspheres in Fig. 2(a) show noticeable core–shell structure of the YSTHSs with a distinguishable inner sphere and thin outer shell for each TiO_2 microsphere, a so-called "yolk-shell" structure. The detailed microstructure of these yolk-shell TiO_2 hierarchical microspheres (YSTHSs) were further investigated by TEM shown in Fig. 2(b)–(c). It was clearly shown in Fig. 2(b) that besides of the outer shell of the YSTHSs, the inner sphere is also clearly observed, which further confirms the yolk-shell structure of these TiO_2 microspheres. Fig. 2(c) displays a TEM image of an individual YSTHS, from which an outer spherical shell with a thickness of approximately 200 nm can be visualized. In addition, the high-resolution SEM image (Fig. 2(d)) reveals that the spherical shell structure of these YSTHSs are assembled by polyhedra TiO_2 nanoparticles with average size of 55 nm (see Table 1). The crystallinity and phase purity of the these YSTHSs were confirmed by XRD (Fig. 2e). As can be seen from the XRD pattern, all the identified diffraction peaks can be well indexed to the data of the standard card of anatase TiO_2 (JCPDS card No. 21-1272). To obtain an insight into the porous structure of these YSTHSs, the N_2 adsorption–desorption isotherms (Fig. 2(f)) was used to determined the pore-size distribution and BET specific surface area of these YSTHSs. BET analysis of the YSTHSs indicates a surface area of 68 m^2 g^{-1} (see Table 1), which is a remarkable large specific surface area for dye adsorption. Moreover, according to the IUPAC classification, the isotherm curve of

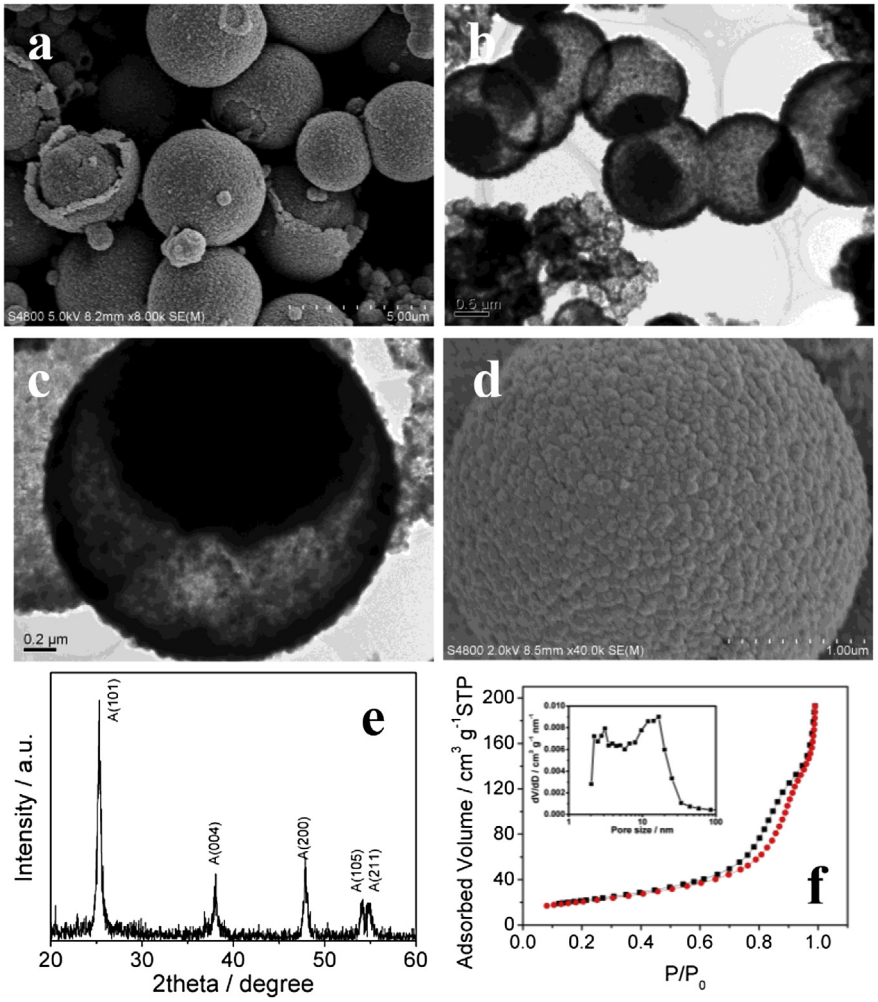

Fig. 2. SEM images of the mesoporous YSTHSs (a) and a magnified SEM image of an YSTHS (d). TEM images of the YSTHSs (b) and of an individual YSTHS (c). (e) XRD pattern of the YSTHSs. (f) N_2 adsorption–desorption isotherms and the corresponding pore size distribution (inset) of the YSTHSs.

Table 1
Physiochemical properties of the prepared YSTHS and P25 (TiO_2).[a]

Samples	S_{BET}($m^2\ g^{-1}$)	APS(nm)	ACS(nm)
P25	51	25	29
YSTHS	68	19	55

[a] ACS – average crystallite size; S_{BET} – BET surface area; APS – average pore size.

Table 2
Comparison of photovoltaic and dye-loading properties of the DSSCs with different photoanodes.

Samples	Thickness (um)	J_{sc} (mA cm^{-2})	V_{oc} (mV)	FF	η (%)	Dye adsorption ($\times 10^{-7}$ mol cm^{-2})
2T	12.4	12.86	680	0.59	4.99	1.542
T-STP	12.6	14.02	680	0.59	5.31	1.226
T-YSTHS	12.8	16.35	679	0.57	6.01	1.767

the YSTHSs belongs to the typical type IV, indicating the mesoporous structure of YSTHSs [30]. Clearly, two salient peaks of 3 nm and 12 nm in the pore size distribution curve (see the inset of Fig. 2(f)) calculated from the adsorption branch of the nitrogen isotherm by the BJH method are observed, which might be related to the different porous structures of yolk and shell [11,31]. Due to the mesoporous structure and relatively high specific surface area in the unique structure of the YSTHSs, more dye loading can be expected in them. Furthermore, such sphere (inner) in shell (outer) nested structure enables multiple light reflection and scattering in-between the hierarchical spheres and spherical shells (see Fig. 1(b)), which would improve the LHE and thus DSSCs efficiency. For the above merits, such YSTHSs are expected to be a promising photoanode material for promoting the DSSCs performance.

3.2. Diffused reflectivity of the photoanode films

It is well accepted that the enhancement of light scattering of TiO_2 photoanode films is crucial for boosting the LHE and then the photoelectric conversion efficiency of DSSCs [8,11,12] To study the light scattering efficiency of the as-prepared photoanode films, their diffuse reflection properties was evaluated. As shown in Fig. 3(a), the reflectances of both T-STP and T-YSTHS films are much higher than that of the conventional nanocrystalline TiO_2 film (2T) in the visible and near-infrared regions, indicating a better light scattering cabability of the bilayer photoanodes. In the case of T-STP photoanode, this enhancement in scattering ability can be attributed to the scattering effect of the large particles in the STP overlayer, for the particle size is comparable to the wavelengths of incident light [32]. While, for the T-YSTHS photoanode, besides that the large size of the YSTHSs play an important role in enhancing light scattering, their unique yolk-shell structure are helpful in confining the incident light within the photoanode by light scattering in-between the inner spheres and the outer spherical shell. Since a real DSSC contains dye-loaded pohotoanode, the reflectance spectra of the dye-sensitized photoanodes were also measured as shown in Fig. 3(b). As can be seen in Fig. 3(b), the reflectances of both the T-YSTHS and 2T films decrease dramatically in the short wavelength region ranging from 400 to 650 nm, which is mainly due to light absorption by the dye molecules. While, the T-STP film still shows a high reflectance at the same wavelength region because of the low light absorption due to low dye-loading (see Table 2). In the long wavelength region, the T-YSTHS film exhibits a substantially higher reflectance than the 2T film and its reflectivity is close to that of the T-STP film.

3.3. Influences of the YSTHSs on the performance of the DSSCs

A cross-section image of the heterostructure bilayer photoanode consisting of the conventional TiO_2 nanocrystalline underlayer and the YSTHS scattering layer is shown in Fig. 4(a). The structure and morphology of the mesoporous YSTHSs were well preserved in the photoanode (see Fig. 4(b)). A dense surface morphology of the underlayer nanocrystalline TiO_2 film is shown in Fig. 4(c). Table 2 compares the photovoltaic performance and the dye adsorption characteristics of DSSCs fabricated with 2T, T-STP and T-YSTHS photoanodes. The typical photocurrent density–voltage (J–V) characteristics and IPCE spectra of these DSSCs are presented in Fig. 5(a) and Fig. 5(b), respectively. As can be seen from the J–V curves, the short-circuit current density (J_{sc}) exhibited a significant and systematic change in the DSSCs with different photoanodes. The DSSC with conventional 2T photoanode had the smallest J_{sc} and PCE (Table 2). Compared with the conventional DSSC, a sigificant increase in the J_{sc} and the PCE were obtained in the DSSC with T-STP photoanode due to the introduce of the STP scattering layer. Due to the relative low specific surface area and the dye adsorption(Table 2), this conventional STP scattering layer serves only to enhance light scattering to enhance light harvest efficiency [20,33]. Therefore, the improved photovoltaic performance of T-STP based DSSC can be understood as a result of improved LHE by enhanced light scattering, which is consistent with the diffused reflectance spectra (Fig. 3). Encouragingly, the novel bilayer photoanode (T-YSTHS) based DSSC exhibited the maximum J_{sc} of 16.35 mA cm^{-2} and PCE of 6.01%, remarkably higher than those of the conventional 2T-based DSSC by 27.1% and 20.4%, respectively. These J_{sc} and PCE values are also significantly higher than those of the T-STP-based DSSC. Evidently, the remarkable enhancement in J_{sc} and PCE for the T-YSTHS-based DSSC compared to the 2T- and T-STP-based DSSCs are mainly attributed to the significant enhancement in light scattering and the increase in dye-loading due to the increase in specific surface area of the YSTHSs (see Fig. 3 and Table 2). Moreover, the dye adsorption capacity for T-YSTHS photoanode (Table 2)

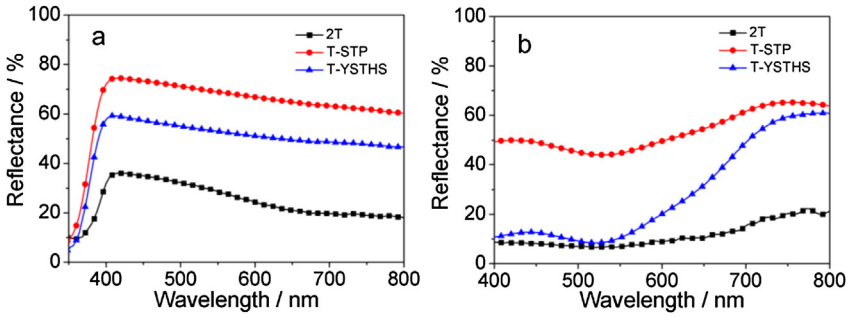

Fig. 3. Diffused reflectance spectra of 2T, T-STP and T-YSTHS photoanode films without (a) and with (b) adsorbed N719 dye.

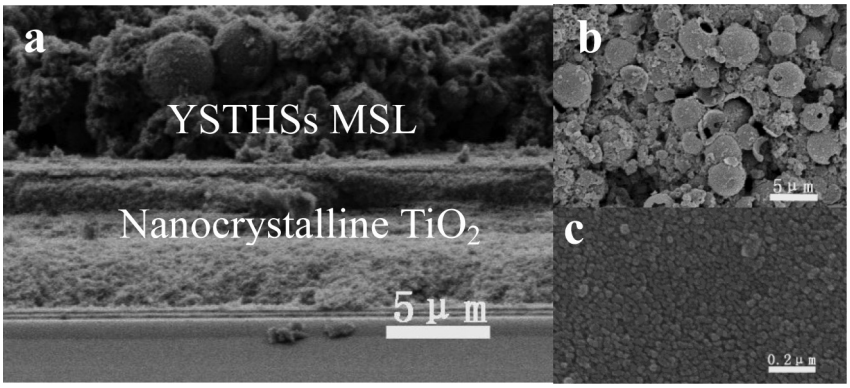

Fig. 4. SEM images of (a) the cross section of T-YSTHS, (b) the surface of the scattering layer composed of mesoporous YSTHSs, (c) the surface of the underlayer nanocrystalline TiO_2 film.

is 1.767 × 10^{-7} mol cm^{-2}, about 44% larger than that of the T-STP. Consequently, considering that the light reflectance of the T-YSTHS photoanode is a little lower than that of the T-STP one (Fig. 3), the higher J_{sc} observed for the T-YSTHS based DSSC than T-STP one is ascribed to the larger quantity of dye loaded on the T-YSTHS photoanode. In addition, we further investigated the dark current–voltage curves of the DSSCs with different photoanodes as shown in the inset of Fig. 5(a). As we know, the dark current–voltage characteristics of the DSSCs reflect, to some extent, the recombination level of the back-transfer photogenerated electrons with triiodide (I_3^-) [34]. As can be seen in the inset of Fig. 5(a), compared with the other two DSSCs, the T-YSTHS based DSSC had the smallest dark current at a certain voltage, indicating the lowest electron recombination rate, which is consistent with the *J–V* curves displayed in Fig. 5(a). This less electron recombination would, to some extent, benefit the increase of the J_{sc} and PCE of the DSSC, which might be attributed to the high electron mobility of such yolk-shell hierarchical microspheres of YSTHSs [35].

The IPCE spectra (Fig. 5(b)) of the DSSCs can provide more information on the performance of the DSSCs. As can be seen in Fig. 5(b), both T-STP and T-YSTHS cells showed a considerable increase in IPCE over the entire wavelength region compared to the 2T cell, which correlates well with the aforementioned *J–V* curves (Fig. 5(a)). For the T-STP cell, considering its less dye-adsorption than that of the 2T, thus its IPCE enhancement is mainly attributed to the improved LHE due to the increased light scattering of the STP. In spite of the lower scattering of the T-YSTHS than the T-STP, the T-YSTHS cell had a higher IPCE than the T-STP based cell because of the remarkable higher dye adsorption of T-YSTHS than that of T-STP (Table 2). As forementioned, such T-YSTHS photoanode has the multifunctions of higher specific surface area than the T-STP photoanode for more dye adsorption and higher light-scattering effect than the conventional 2T photoanode, resulting in the highest IPCE and thus the J_{sc} and PCE in the T-YSTHS cell.

Electrochemical impedance spectroscopy (EIS) analysis has been regarded as a powerful tool for investigating the kinetics of electrochemical and photoelectrochemical processes occurring in DSSCs [36]. To better understand the electron transport properties and reveal the difference in the interfacial characteristics of the DSSCs with 2T, T-STP and T-YSTHS phtoanodes, EIS was carried out, as illustrated in Fig. 6. In each of the EIS spectra, two semicircles were clearly observed in the high frequency region (>1 kHz, small one Z_1) and in the mid-frequency region of 100–1 Hz (large one Z_2), respectively. The smaller semicircle in the high frequency region reflects charge transport at the TiO_2/conducting layer or Pt/electrolyte interfaces (Z_1), while the larger one denotes the charge transfer at the TiO_2/dye/electrolyte interface (Z_2) [37]. Table 3 summarizes the results of the EIS analysis fitted by an equivalent circuit (the inset of Fig. 6(a)) containing resistances (R) and constant phase elements (CPE) by using the commonly used "Zview" software [38,39]. Since all the FTO and the Pt counter electrodes used in our DSSCs were identical, the influences of Z_1 can be ignored. Therefore, our main concern, here, is focused on the TiO_2/dye/electrolyte interface transfer resistance R_2 (real part of Z_2). From the Nyquist plots in Fig. 6(a), we could see that the diameter of Z_2 for the DSSC with T-YSTHS photoanode was the smallest among the three DSSCs, resulting in the smallest value (11.3 Ω) of R_2. The smaller the value of R_2, the less recombination reaction of electrons with triiodide ions and the excited dye at the TiO_2/dye/electrolyte interface, and thus a enhanced J_{sc} [40]. Therefore, the largest J_{sc} was achieved in the T-YSTHS based DSSC compared to other two DSSCs, which was in good agreement with the *J–V* characteristics.

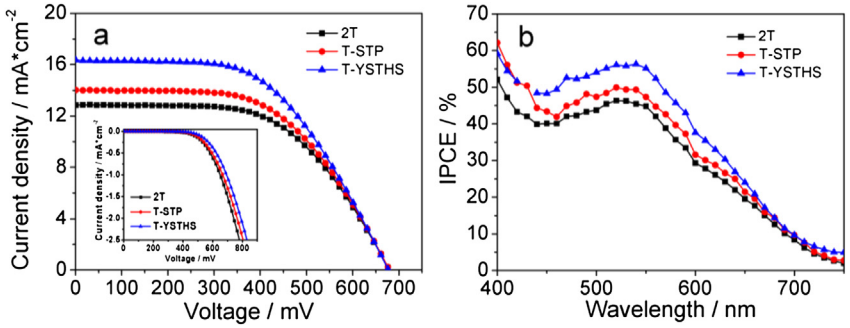

Fig. 5. *J–V* curves (a) and IPCE spectra (b) of DSSC devices based on 1T, 2T, T-STP, and T-YSTHS photoanodes. The inset is the corresponding dark current characteristics.

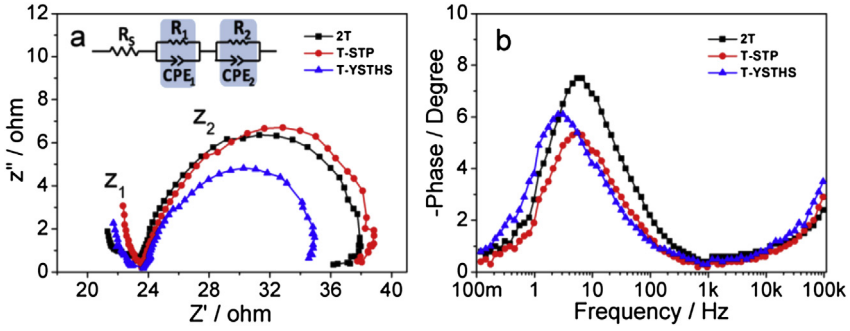

Fig. 6. Nyquist plots (a) and bode impedance plots (b) of the DSSCs with the 2T, T-STP and T-YSTHS photoanodes. The inset in (a) shows the equivalent circuit.

Table 3
Fitting results derived from EIS analysis.

Samples	$R_2(\Omega)$	f_{max}(HZ)	τ_e(ms)
2T	14.4	4.54	35.06
T-STP	15.3	4.59	34.67
T-YSTHS	11.3	2.55	62.41

Electron lifetime (τ_e) in DSSCs can be estimated from the peak frequency (f_{max}) of the mid-frequency semicircle according to the relationship: $\tau_e = 1/2\pi f_{max}$ [41]. From the Bode phase plots in Fig. 6(b), it is noted that the f_{max} of the DSSC with T-YSTHS photoanode shifted to the lowest frequency (2.55 Hz, Table 3) relative to the other two DSSCs, corresponding to the longest electron lifetime τ_e of 62.41 ms. This suggests that the more fluently transportation, the less recombination of the photoelectrons and thus the enhanced J_{sc} in the T-YSTHS based DSSC, which can be attributed to the high electron mobility in the unique york-shell structure of the YSTHS [35,42].

4. Conclusions

In conclusion, unique mesoporous YSTHSs with a yolk-shell hierarchical microsphere structure are successfully prepared via a simple one-pot hydrothermal method. A novel DSSC assembled with a heterostructure bilayer photoanode consisted of a YSTHS overlayer and a conventional TiO_2 nanocrystalline underlayer (T) was prepared. Influences of the unique structure of the YSTHS on the properties of the photoanode and the DSSC were investigated. Studies indicated that, by introducing the YSTHS overlayer to form a novel bilayer T-YSTHS photoanode, the light scattering of the photoanode was greatly enhanced, and the dye adsorption as well as the electron mobility and lifetime were increased, and thus the J_{sc} and PCE were remarkably increased. This T-YSTHS based DSSC exhibited the maximum J_{sc} of 16.35 mA cm^{-2} and PCE of 6.01%, remarkably higher than those of the 2T-based DSSC by 27.1% and 20.4%, respectively. These J_{sc} and PCE values are also significantly higher than those of the T-STP-based DSSC. The remarkable enhancement in J_{sc} and PCE for the T-YSTHS-based DSSC compared to the 2T- and T-STP-based DSSCs are mainly attributed to the significant enhancement in light scattering and the increase in dye-loading due to the increase in specific surface area arised from the unique yolk-shell hierarchical structure of the YSTHSs.

Acknowledgments

This work was supported by the National Basic Research Program of China (Grant No.: 2011CB933304), the National Natural Science Foundation of China (Grant No.: J1210061) and the Fundamental Research Funds for the Central Universities (Grant No.: 20102020101000036).

References

[1] B. Oregan, M. Grätzel, Nature 353 (1991) 737–740.
[2] M. Grätzel, Nature 414 (2001) 338–344.
[3] M.K. Nazeeruddin, R. Humphry-Baker, P. Liska, M. Grätzel, J. Phys. Chem. B 107 (2003) 8981–8987.
[4] A. Yella, H.W. Lee, H.N. Tsao, C.Y. Yi, A.K. Chandiran, M.K. Nazeeruddin, E.W.G. Diau, C.Y. Yeh, S.M. Zakeeruddin, M. Grätzel, Science 334 (2011) 629.
[5] R.A. Caruso, J.H. Schattka, A. Greiner, Adv. Mater. 13 (2001) 1577–1579.
[6] Y.G. Guo, Y.S. Hu, J. Maier, Chem. Commun. 26 (2006) 2783.
[7] G.K. Mor, K. Shankar, M. Paulose, O.K. Varghese, C.A. Grimes, Nano Lett. 6 (2006) 215.
[8] D.H. Chen, F.Z. Huang, Y.B. Cheng, R.A. Caruso, Adv. Mater. 21 (2009) 2206–2210.
[9] B. Liu, E.S. Aydil, J. Am. Chem. Soc. 131 (2009) 3985–3990.
[10] Z.B. Lv, J.F. Yu, H.W. Wu, J. Shang, D. Wang, S.C. Hou, Y.P. Fu, K. Wu, D.C. Zou, Nanoscale 4 (2012) 1248–1253.
[11] J.G. Yu, J.J. Fan, K.L. Lv, Nanoscale 2 (2010) 2144–2149.
[12] Y.M. Liu, H.W. Zhai, F. Guo, N. Huang, W.W. Sun, C.H. Bu, T. Peng, J.K. Yuan, X.Z. Zhao, Nanoscale 4 (2012) 6863–6869.
[13] A.K. Chandiran, F. Sauvage, L. Etgar, M. Grätzel, J. Phys. Chem. C 115 (2011) 9232–9240.
[14] H.J. Tian, L.H. Hu, W.X. Li, J. Sheng, S.Y. Xu, S.Y. Dai, J. Mater. Chem. 21 (2011) 7074–7077.
[15] X.L. Fang, M.Y. Li, K.M. Guo, Y.D. Zhu, Z.Q. Hu, X.L. Liu, B.L. Chen, X.Z. Zhao, Electrochim. Acta 65 (2012) 174–178.
[16] J.N. Clifford, E. Palomares, M.K. Nazeeruddin, R. Thampi, M. Grätzel, J.R. Durrant, J. Am. Chem. Soc. 126 (2004) 5670–5671.
[17] Y.Z. Wu, X. Zhang, W.Q. Li, Z.S. Wang, H. Tian, W.H. Zhu, Adv. Energy. Mater. 2 (2012) 149–156.
[18] S. Hore, P. Nitz, C. Vetter, C. Prahl, M. Niggemann, R. Kern, Chem. Commun. 15 (2005) 2011–2013.
[19] M. Gratzel, Inorg. Chem. 44 (2005) 6841.
[20] F.Z. Huang, D.H. Chen, X.L. Zhang, R.A. Caruso, Y.B. Cheng, Adv. Funct. Mater. 20 (2010) 1301–1305.
[21] J.G. Yu, S.W. Liu, M.H. Zhou, J. Phys. Chem. C 112 (2008) 2050–2057.
[22] J.H. Pan, X.W. Zhang, A.J. Du, D.D. Sun, J.O. Leckie, J. Am. Chem. Soc. 130 (2008) 11256–11257.
[23] S.W. Liu, J.G. Yu, S. Mann, Nanotechnology 20 (2009) 325606.
[24] A.F. Demirors, A.V. Blaaderen, A. Imhof, Langmuir 26 (2010) 9297–9303.
[25] J. Liu, S.Z. Qiao, S.B. Hartono, G.Q.M. Lu, Angew. Chem. Int. Ed. 122 (2010) 5101–5105.
[26] Z.Y. Wang, D.Y. Luan, F.Y.C. Boey, X.W. Lou, J. Am. Chem. Soc. 133 (2011) 4738–4741.
[27] A.Q. Pan, H.B. Wu, L. Yu, X.W. L, Angew. Chem. Int. Ed. 125 (2013) 2282–2286.
[28] Z.Y. Wang, Z.C. Wang, W.T. Liu, W. Xiao, X.W. Lou, Energy. Environ. Sci. 6 (2013) 87–91.
[29] K.M. Guo, M.Y. Li, X.L. Fang, X.L. Liu, B. Sebo, Y.D. Zhu, Z.Q. Hu, X.Z. Zhao, J. Power Sources 230 (2013) 155–160.
[30] M. kruk, M. Jaroniec, Chem. Mater. 13 (2001) 3169.
[31] J.S. Chen, D. Luan, C.M. Li, F.Y.C. Boey, S. Qiao, X.W. Lou, Chem. Commun. 46 (2010) 8252–8254.
[32] H.C. van deHulst, Light Scattering by Small Particles, Wiley, New York, 1957.
[33] H.J. Koo, Y.J. Kim, Y.H. Lee, W.I. Lee, K.K. Kim, N.G. Park, Adv. Mater. 20 (2008) 195–199.
[34] K.M. Guo, M.Y. Li, X.L. Fang, X.L. Liu, Y.D. Zhu, Z.Q. Hu, X.Z. Zhao, J. Mater. Chem. A 1 (2013) 7229–7234.
[35] X. Wu, G.Q. Lu, L.Z. Wang, Energy. Environ. Sci. 4 (2011) 3565–3572.
[36] Q. Wang, J.E. Moser, M. Grätzel, J. Phys. Chem. B 109 (2005) 14945–14953.

[37] L. Han, N. Koide, Y. Chiba, T. Mitate, Appl. Phys. Lett. 84 (2004) 2433.
[38] F. Shao, J. Sun, L. Gao, S.W. Yang, J.Q. Luo, J. Phys. Chem. C 115 (2011) 1819–1823.
[39] W.G. Wang, H.Y. Zhang, R. Wang, M. Feng, Y.M. Chen, Nanoscale 6 (2014) 2390–2396.
[40] C.-S. Chou, R.-Y. Yang, C.-K. Yeh, Y.-J. Lin, Powder Technol. 194 (2009) 95–105.
[41] J. Qian, P. Liu, Y. Xiao, Y. Jiang, Y. Cao, X. Ai, H. Yang, Adv. Mater. 21 (2009) 3663–3667.
[42] S.C. Yang, D.J. Yang, J. k. Kim, J.M. Hong, H.G. Kim, I.D. Kim, H.J. Lee, Adv. Mater. 20 (2008) 1059–1064.